6

Adaptive Antenna Arrays for Ad-Hoc Millimetre-Wave Wireless Communications

Val Dyadyuk, Xiaojing Huang, Leigh Stokes, Joseph Pathikulangara, Andrew R. Weily, Nasiha Nikolic, John D. Bunton and Y. Jay Guo
CSIRO ICT Centre
Australia

1. Introduction

New technologies that employ millimetre-wave frequency bands to achieve high speed wireless links are gaining more attention (Dyadyuk et. al., 2007, 2009b, 2010a; Hirata et. al., 2006; Lockie & Peck, 2009; Kasugi et. al., 2009; Wells, 2009) due to increasing demand for wideband wireless communications. Very wide uncongested spectrum is available in the E—bands (71-76 GHz and 81-86 GHz) recently allocated for wireless communications in USA, Europe, Korea, Russia and Australia. The E-band provides an opportunity for line-of – sight (LOS) links with higher data rates, well suited for fibre replacement and backhaul applications.

Future mobile and ad-hoc communications networks will require higher bandwidth and longer range. An ad-hoc or mobile (e.g. inter-aircraft) network that relies on high gain antennas also requires beam scanning. Adaptive antenna arrays have found a wide rage of applications and are becoming essential parts of wireless communications systems (Abbaspour-Tamijani & Sarabandi, 2003; Do-Hong & Russer, 2004; Gross, 2005; Guo, 2004; Krim & Viberg, 1996; Mailloux, 2005, 2007; Rogstad et al., 2003; Singh et al., 2008). While the spectrum available in the millimetre-wave frequency bands enables multi-gigabit-per second data rates, the practically achievable communication range is limited by several factors. These include the higher atmospheric attenuation at these frequencies and limited output power of monolithic microwave integrated circuits (MMIC) (Doan et al., 2004; Dyadyuk et al., 2008a; Kasper et al., 2009; Floyd et al., 2007; Reynolds et. al., 2006; Vamsi et. al., 2005, Zirath et al., 2004) due to physical constraints. Therefore, the performance of the ad-hoc or mobile millimetre-wave networks requires enhancement by using spatial power combining antenna arrays.

Advantages of spatial power combining arrays for long-range high-speed millimetre-wave LOS links are discussed in Section 2. Combining multiple antennas, each of which has its own low noise amplifier (LNA) or power amplifier (PA), to form an antenna array not only increases the communications range but also enables smart antenna technology to be applied to optimize the system performance. The increased transmission power of an antenna array provides an opportunity to realize longer range point-to-point LOS links, such as those providing wireless connectivity between aircraft and/or between aircraft and ground vehicles or control stations.

A proposed hybrid antenna array concept (Guo et. al., 2009; Dyadyuk & Guo, 2009a; Huang et al., 2009) for high-speed long-range millimeter-wave mobile and ad hoc wireless networks is described in Section 3. The hybrid array consists of a number of analogue sub-arrays and a digital beamformer to overcome the space constraint and digital implementation complexity problem for a large array at mm-wave frequencies.
Section 4 formulates the time- and frequency-domain digital beamforming algorithms proposed for the hybrid antenna arrays (Huang et al., 2010a, 2010b) and discusses their relative merits.
Section 5 describes a small-scale prototype that implements an analogue-beam-formed phased antenna array. The prototype (Dyadyuk & Stokes, 2010a) was developed to demonstrate a communications system with gigabit per second data rates in the E-band using an electronically steerable array as an initial step towards fully ad-hoc communications systems that implement hybrid antenna arrays. The steerable beam receiver and a fixed beam transmitter form a prototype of the E-band communication system that implements an adaptive antenna array. The prototype configuration is flexible and can be used for experimental verification of both analogue and digital beam forming algorithms. The main functional block of the prototype is a four-channel receive RF module integrated with a linear end-fire Quasi-Yagi antenna array.
Section 6 describes the design, EM simulations and tests results of a Quasi-Yagi antenna array (Deal et al. 2000; Nikolic & Weily, 2009, 2010) used in the receive RF module described above. Array element spacing was 2 mm (or 0.48 wavelengths at the carrier frequency) to suppress the appearance of grating lobes for scanning angles up to ± 42 degrees.
The test results of the E-band prototype that implements a phased antenna array are given in Section 7. Measured radiation patterns for the analogue beamformed array are presented and compared with EM simulation predictions. Beam steering accuracy of 1 degree has been achieved with 6-bit digital phase shift and magnitude control at IF. A small ad-hoc point-to-point link has also been tested with reasonable Bit Error Rate (BER) measured for selected angles using 8PSK modulation at 1.5Gbps data rate with the receive array beam formed in the direction of arrival of the transmitted signal. Digital beamforming experiments have also been conducted on this prototype using a wideband frequency-domain algorithm showing antenna array patterns very close to those obtained with analogue beamforming and simulations. A quantitative analysis of the digital beam forming results is beyond the scope of this chapter and can be found in Dyadyuk et al., 2010c; Huang et al., 2010b.
Finally, conclusions are drawn in Section 8. Analytical results were experimentally verified using a steerable receive array demonstrator in the E-band.
The future research objectives and challenges of practical implementation of large adaptive millimetre-wave antenna arrays have also been addressed. This work represents a stepping stone towards realisation of high-data rate millimetre-wave communication systems employing hybrid antenna arrays.

2. Spatial power combining arrays at mm-wave frequencies

With the advance in digital signal processing techniques, the adaptive antenna array is becoming an essential part of wireless communications systems (Guo, 2004; Mailoux, 2005). The use of adaptive antenna arrays for long range millimeter wave ad-hoc communication networks is particularly critical due to increased free space loss and reduced level of practically achievable output power relative to those available in lower frequency bands. An

ad-hoc or mobile network that relies on high gain antennas also requires beam scanning. The antenna beam can be steered to a desired direction with appropriate beam forming. Passive phased arrays generally suffer from losses in combining networks that are very high at the mm-wave frequencies.

In a spatial power-combining phased array transmitter, each individual element has a power amplifier (PA). To generate a pencil beam in a particular direction, the signal radiated from each element is delayed electronically in order to compensate for differences in the free-space propagation time from the different elements. In a spatial power-combining transmitter with multiple radiating elements, this coherent addition increases the Effective Isotropic Radiated Power (EIRP) in two ways: firstly via the increase in directivity due to the increased electrical aperture; and secondly, via the increase in total radiated power through the increased number of power amplifiers. So if we take the efficiency of the spatial power combining transmitter to be η, for an array of N elements, each generating an EIRP of P watts, the EIRP of the transmitter is $\eta N^2 P$ watts. Assuming an efficiency of 100%, the increase in EIRP in going from 1 to N elements is 20 $log(N)$ dB. These results are plotted in Figure 1, where the equivalent EIRP of passive and active arrays is plotted versus number of array elements.

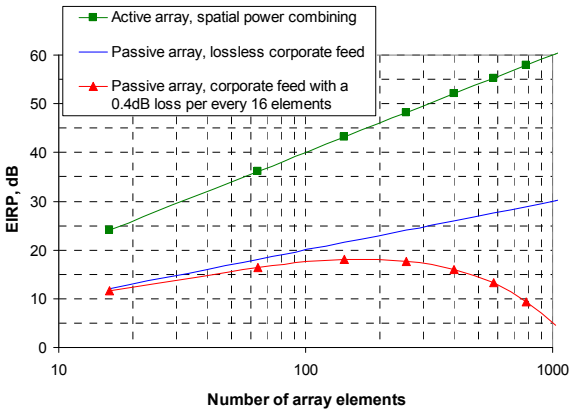

Fig. 1. Active versus passive phased array transmitters

It should be noted that the data for a lossless corporate feed plotted in Fig. 1 is a theoretical assumption only. It does not take into account the power combining loss for the passive array with a single PA. The combining loss is hard to predict as it largely depends on number of elements, operating frequency and other parameters of a specific design, and could be in the order of several dB. An example shown in Fig. 1 that uses an optimistic assumption of only 0.4dB loss per every 16-element block (e.g., 0.1 dB per stage using a binary combining structure) illustrates a low efficiency of passive power combining. Thus, EIRP is rapidly reduced for a moderate-size array (when the number of element is more that 300), and larger passive arrays would be impractical.

Where the receive terminal is equipped with an identical antenna array having a low noise amplifier associated with each element, the effective SNR increases proportionally to N^3 or more (due to reduction of the effective receiver noise dependent on the degree of the correlation).

To achieve wide bandwidth with a phased array requires detailed calculation of mutual coupling between elements, since this determines the impedance match at each element and the radiation pattern of the complete array, and these two are interrelated. The apparent impedance match at each element can vary widely as the main beam is scanned. In general, the array bandwidth is limited by array considerations that are directly related to the array element size, and the impedance bandwidth of an isolated array element, which is also related to the element size by basic electromagnetic considerations.
For a directly-radiating phased array, the element spacing is determined by the need to suppress grating lobes, that is, additional main lobes in the radiation pattern of the array. For a linear phased array with the main beam scanned at an angle θ_0 from broadside, the equation for grating lobes is easily determined (Mailloux, 2005) as:

$$\frac{d}{\lambda} = \frac{k}{\sin\theta_0 - \sin\theta_{gl}} \tag{1}$$

where d_s is the array spacing, λ is the wavelength, θ_{gl} is the angle of the grating lobe and k is the order of the grating lobe. If the maximum scan angle is taken to be θ_0, then we can suppress the appearance of grating lobes so long as the array element spacing satisfies the condition for the smallest operating wavelength λ_{min}:

$$\frac{d_s}{\lambda_{\min}} \le \frac{1}{1+\sin\theta_0} \tag{2}$$

For a uniform square lattice array with element size equal to the element spacing d_s, the ratio of upper to lower operating frequency is related to the maximum scan angle by:

$$\frac{f_{\max}}{f_{\min}} = \frac{d_s}{1+\sin\theta_0} \tag{3}$$

Thus for larger, wideband elements the bandwidth is limited by array effects, whereas for small, resonant elements, the element bandwidth typically restricts the overall array bandwidth. In an ideal broadband phased array, a high-gain pencil beam is generated by a true time delay at each element that compensates exactly for the free-space propagation delay. Developing a low-loss, linear delay line directly at mm-wave frequencies is very challenging. Equivalent delay can also be implemented by delay/phase-shift in the IF and LO channels, or implemented digitally. For a relatively narrow-band system, implementing the delay as an equivalent phase shift at the centre frequency is a simple option, and then many of the problems of mm-wave phase shifters can be avoided by implementing the phase shift directly on the IF or LO. When an array is scanned with phase shift instead of true time delay, the position of the main beam varies with frequency, and this effect becomes more pronounced the further the beam is scanned from the array normal. To calculate the array bandwidth, a common definition used is to define the upper and lower frequencies of the band as the frequencies where the main beam has moved from the desired scan angle to the 3dB points of the beam. Then, for a large uniform array, the fractional bandwidth B is given by:

$$B \approx \frac{0.866\,\lambda}{D\sin\theta_0} \tag{5}$$

where D is the array diameter, and θ_0 is the maximum scan angle. The corresponding gain G at the maximum scan angle is related to the physical area A by:

$$G \approx \eta \frac{4\pi}{\lambda^2} A \cos\theta_0 \tag{6}$$

where η is the efficiency.

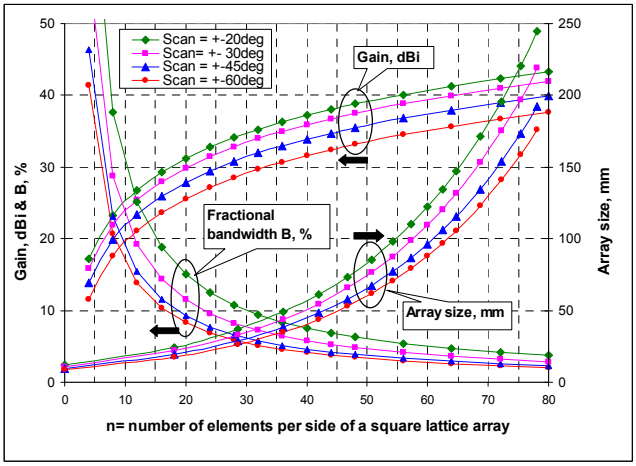

Fig. 2. Array gain, size and fractional bandwidth calculated for selected scan angles at for a centre frequency of 73GHz

At the mm-wave frequencies, phase-only beam steering becomes practical for this type of transmitting array since the size of a high EIRP array remains moderate. This is illustrated in Fig. 2 where the square lattice array gain, size and fractional bandwidth are calculated at the centre frequency of 73 GHz using equations (1 – 6) and assuming a maximum scan angle of 60 degrees, and an efficiency of 1. It can be noted that for a 1000-element array, the fractional bandwidth exceeds 7% at the scan angles within ±45°. This allows for a phase-only beam steering over the full 5 GHz wide RF channels available in the E-band.

3. Hybrid antenna array

Small size, high EIRP active antenna arrays would be suitable for long range inter-aircraft communications as atmospheric attenuation at millimeter-wave frequencies is low at elevated altitudes (above the rain height). Figure 3a shows the predicted communication range for a point-to-point link (Dyadyuk et al., 2010a) equipped with active square lattice $N=n^2$ element arrays. Operating frequency is 73GHz, transmit power is 15 dBm per array element, reference atmospheres and other link specification details are available in Dyadyuk et al., 2010a.

There are two major technical problems to be solved for practical realisation of such systems: the tight space constraints and beamforming complexity. As antenna elements must be spaced closely together to prevent grating lobes, array element spacing is extremely small (about 2 mm in the E-band) as illustrated in Fig. 3b.

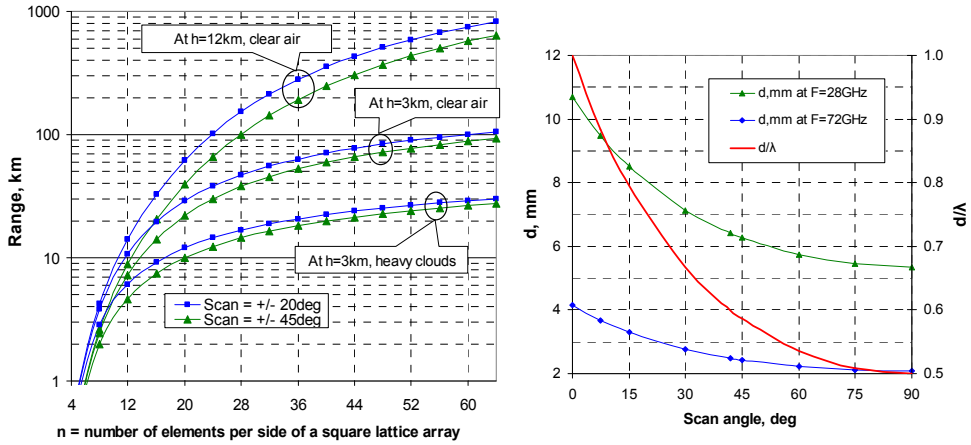

a) b)

Fig. 3. a) Predicted range of a PTP link equipped with active antenna arrays calculated for 1GHz bandwidth, centre frequency of 73GHz and transmitted power of 15 dBm per element; b) Theoretical maximum array element spacing

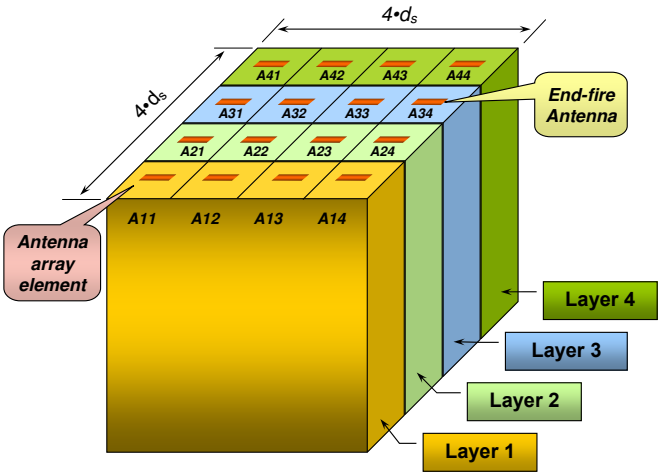

Fig. 4. Configuration of a 4x4 element square lattice sub-array. Each "layer" represents a four-element sub-module integrated on a common printed circuit board

The RF front end components, such as the low noise amplifier (or power amplifier), frequency converter, local oscillator (LO), as well as the intermediate frequency (IF) or baseband circuitry in the analogue signal chain should be tightly packed behind the antenna elements. Difficulties of integration of the RF front end components can be illustrated on a simple example of a commercial GaAs low noise amplifier ALH459 available from Hittite Microwave (Velocium product line). While the width of a bare die is 1.6mm, an additional space needed to accommodate the DC bias circuitry (using single-layer ceramic capacitors

and resistors) increases the width to 3.5-3.7 mm, which is greater than the maximum antenna element spacing required. Although there has been a rapid progress in the CMOS and SiGe technology for the mm-wave applications (Cathelin et al., 2007; Floyd et al., 2007; Grass et al., (2007); Laskin et al., 2007; Pfeiffer et al., 2008; Reynolds et al., 2007) and advanced multi-chip module integration technologies (Posada et al., 2007), GaAs MMIC are likely to be a preferable technology for the E-band low noise and power amplifiers for some years to come.
A schematic representation of a configuration of a 4 by 4 element sub-array with element spacing d_s is shown in Fig. 4. End-fire antenna array elements are preferable to broadside elements for a planar integration of the antenna elements with the RF chains.

Thus, the area of a 4 by 4 sub-array with IF beam forming implemented in the E-band is about 100 mm^2 (d_s =2.5mm) and it would provide a tight, but feasible accommodation for each the IF, LO, power and control circuits. An arrangement shown in Fig. 4 allows for staggered placement of the adjacent MMICs within each layer. A number of such analogue sub-arrays can be controlled by a digital beam former to form a hybrid antenna array.

4. Beamforming algorithms for a hybrid adaptive array

Since the antenna elements in an array must be placed close together to prevent grating lobes, the analogue components, such as the LNA or PA and the down or up converter associated with each antenna element, must be tightly packed behind the antenna element. This space constraint appears to be a major engineering challenge at mm-wave frequencies. For example, at 74 GHz frequency, the required element spacing is only about 2 mm. With the current MMIC technology, the practical implementation of such a digital antenna array remains very difficult (Doan et al., 2004; Rogstad et al., 2003). Another issue with pure digital beamformers is the excessive demand on real time signal processing for high gain antennas. To achieve an antenna gain of over 30 dBi, for instance, one may need more than 1000 antenna elements. This makes most beamforming algorithms impractical for commercial applications. Furthermore, to perform wideband digital beamforming, each signal from/to an antenna element is normally divided into a number of narrow-band signals and processed separately, which also adds to the cost of digital signal processing significantly. Therefore, a full digital implementation of large, wideband antenna arrays at mm-wave frequencies is simply unrealistic (Gross, 2005). Finally, although multipath is not a major concern for the above mentioned LOS applications, the relative movement between transmitters and receivers will bring other technical challenges such as fast Doppler frequency shift and time-varying angle-of-arrival (AoA) of the incident beam.
A novel hybrid adaptive receive antenna array is proposed using a time-domain (Huang et al., 2009) and frequency-domain (Huang et al., 20010b; Dyadyuk et al., 2010c) approaches to solve the digital implementation complexity problem in large arrays for long range high data rate mm-wave communications. In this hybrid antenna array, a large number of antenna elements are grouped into analogue sub-arrays. Each sub-array uses an analogue beamformer to produce a beamformed sub-array signal, and all sub-array signals are combined using a digital beamformer to produce the final beamformed signal (Guo et al., 2009). Each element in a sub-array has its own radio frequency (RF) chain and employs an analogue phase shifting device at the intermediate frequency (IF) stage. Signals received by all elements in a sub-array are combined after analogue phase shifting, and the analogue

beamformed signal is down-converted to baseband and then converted into the digital domain. In this way, the complexity of the digital beamformer is reduced by a factor equal to the number of elements in a sub-array. For example, for a 1024 element hybrid array of 64 sub-arrays each having 16 elements, only 64 inputs to the digital beamformer are necessary, and the complexity is reduced to one sixteenth for algorithms of linear complexity, such as the least mean square (LMS) algorithm. The cost of the digital hardware is also significantly reduced.

The digital beamformer estimates the AoA information to control the phases of the phase shifters in the analogue sub-arrays and also adjusts the digital weights applied to the sub-array output signals to form a beam. Sub-array technology has been used over the past decades (Abbaspour-Tamijani & Sarabandi, 2003; Goffer et al., 1994; Haupt, 2007; Mailloux, 2005, 2007). Prior ideas include employing a time delay unit to each phased sub-array for bandwidth enhancement, and eliminating phase shifters in the sub-array for applications requiring only limited-field-of-view.

The proposed hybrid antenna array concept differs in that it is a new architecture allowing the analogue sub-arrays and the low complexity digital beamformer to interact with each other to accommodate the current digital signal processing capability and MMIC technology, thus enabling the implementation of a large adaptive antenna array. Two time-domain Doppler-resilient adaptive angle-of-arrival estimation and beamforming algorithms were proposed (Huang et al., 2009) for two configurations of sub-arrays: the interleaved and the side-by-side sub-array. The formulated differential beam tracking (DBT) and the differential beam search (DBS) algorithms have been evaluated. Simulations based on a 64 element hybrid planar array of four 4 by 4 element subarrays were used to evaluate the DBT and DBSD algorithms performance. Recursive mean square error (MSE) bounds of the developed algorithms were also analyzed.

The DBT algorithm was proposed for the hybrid array of interleaved sub-arrays. It does not have a phase ambiguity problem and converges quickly. The DBS algorithm was proposed for the side-by-side sub-arrays. It scans all the possible beams to solve the phase ambiguity problem, but it converges slowly. Both the DBT and DBS algorithms require the computation of sub-array cross-correlations in the time-domain. For practical implementation reasons, a hybrid antenna array of side-by-side sub-arrays is preferable.

Performing AoA estimation and beam forming in the frequency-domain would significantly reduce the implementation complexity and also mitigate the wideband effects on the hybrid array. A frequency-domain beamforming algorithm has been proposed and successfully evaluated on a small-scale linear array demonstrator. Simulation results show that the performance of the proposed algorithms is dependent on the fractional bandwidth of the hybrid array. Detailed description of the digital beamforming algorithms can be found in Dyadyuk et al., 1010c; Huang et al., 2010b. The remainder of this chapter will focus on the analogue sub-array as a part of a hybrid array.

5. Ad-hoc communication system prototype

5.1 System block diagram

The prototype has been developed to demonstrate a communications system with gigabit per second data rates using an electronically steerable array as an initial step towards fully ad-hoc communications systems. The prototype configuration is flexible and can be used for experimental verification of both analogue and digital beam forming algorithms. The

scannable beam receiver and a fixed beam transmitter form a prototype of the E-band communication system that implements an adaptive antenna array. Block diagram Fig. 5 shows the configuration for analogue beam forming experiments.

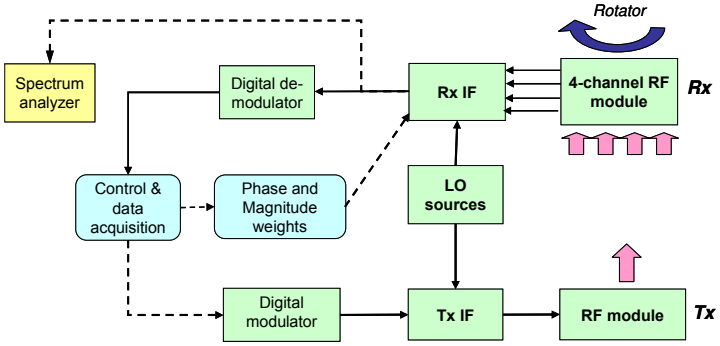

Fig. 5. Block diagram of the E-band communication system that implements a steerable receive antenna array

The receive RF module is mounted on a rotator providing mechanical steering in the azimuth plane for the array pattern measurement. Both the receiver and transmitter use dual frequency conversion with the baseband (IF2) frequency 1 – 2 GHz that enables re-use of the digital modulator and demodulator reported earlier in Dyadyuk et al., 2007.

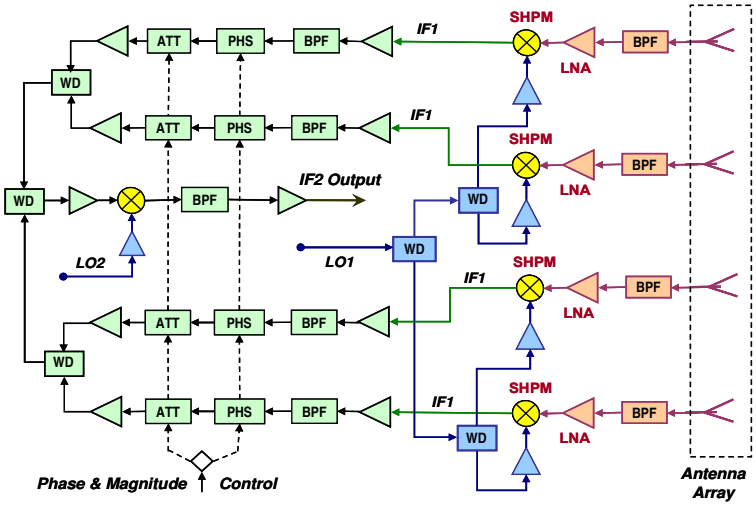

Fig. 6. Simplified schematic of the E-band steerable receive array configured for analogue beam-forming

The receive IF module (Rx IF) has been developed in two versions. In the digital beam forming configuration, each of the IF channels is connected to a digital beam former that replaces the de-modulator. For the analogue beam forming configuration all IF outputs are combined before de-modulation as shown in Fig. 6 where BPF, LNA, SHPM, WD, PHS and

ATT denotes a band-pass filter, low noise amplifier, sub-harmonically pumped mixer, Wilkinson divider, phase shifter and attenuator respectively.
Phase and magnitude controls for each channel are implemented at IF using 6-bit digital phase shifters HMC649LP6 and attenuators HMC4214LP3 available from Hittite Microwave Corporation. They are used to equalize the channels frequency responses (initial calibration) and to apply required beam forming weights.
A single channel transmit module has been built using the up-converter (Dyadyuk et al., 2008a) that uses a sub-harmonically pumped (SHPM) GaAs Schottky diode mixer (Dyadyuk et al., 2008b) with an addition of a commercial band-pass filter and a medium power amplifier, and a corrugated horn antenna with the gain of 22.5 dBi. Measured to the antenna input of the RF transmitter (Dyadyuk & Guo, 2009), the small signal conversion gain and the output power at -1 dB gain compression was 35±1 dB and +15±1 dBm respectively over the operating frequency range of 71.5 – 72.5 GHz.

5.2 RF module of a steerable receive array

The main functional block of the prototype is a four-channel dual-conversion receive RF module integrated with a four-element linear end-fire quasi-Yagi antenna array described below in Section 6. Figure 7 shows a photograph of the assembled RF module (a) and typical measured conversion gain for each channel (b).

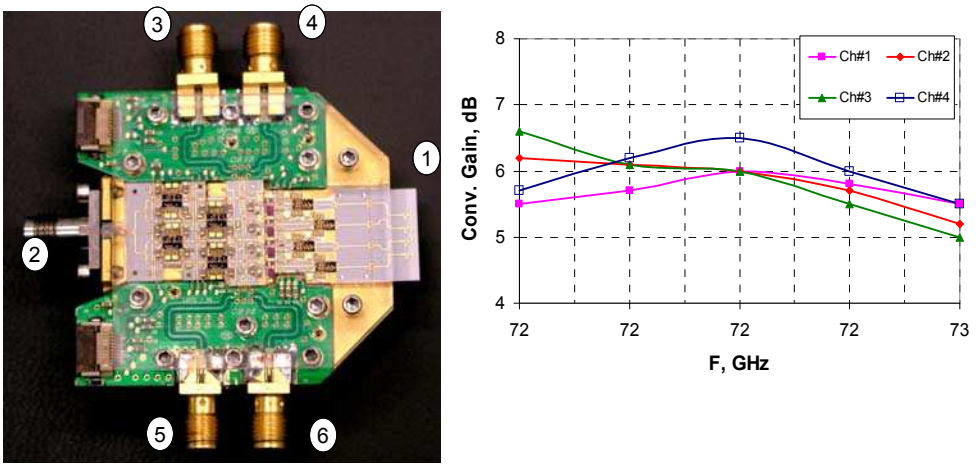

a) b)

Fig. 7. a) Photograph of the RF module assembly where: 1 is the antenna array; 2 is the LO input; 3-6 are IF outputs; b) Typical measured conversion gain (RF to IF1) for each channel

The RF module uses sub-harmonic frequency converters (Dyadyuk et al., 2008b) at the LO frequency of 38 GHz. For each channel we have used a combination of CSIRO and commercial-off the-shelf MMICs similar to those reported earlier for a single-channel receiver (Dyadyuk et al., 2008a). The IF pre-amplifiers, interconnect, matching, and group delay equalization circuits have been developed using a standard commercial thin-film process on ceramic substrate. It includes 16 MMICs, 12 types of microwave boards (on 127um Alumina substrate), 140 microwave passives, and about 400 wire-bond connections.

The receiver is usable over the frequency range of 71 to 76 GHz at the sub-harmonic LO of 38 to 39 GHz and intermediate frequency 1 to 7 GHz. Typical conversion gain was 6 ± 1 dB over the operating RF and IF frequency range of 71.5 -72.5 GHz and 3.5 -4.5 GHz respectively. The maximum magnitude imbalance between each of four channels was below ± 1.5 dB.

6. Quasi-Yagi antenna and linear array for E-band applications

This section of the chapter describes a single quasi-Yagi antenna element and four-element linear arrays designed to operate in the 71-76 GHz band, using planar microstrip technology. Four linear arrays, each containing four elements and having a different beamforming network are designed, fabricated and tested. For testing of the arrays, a suitable microstrip-to-waveguide transition was designed and its calculated reflection coefficient and transmission loss are included. The simulated results for a single element and the measured and simulated reflection coefficient, radiation patterns and gain for each array are presented.

6.1 Quasi-Yagi element

The element used to design the array is based on the antenna presented in Kaneda et al., 1998; Deal et al., 2000; Kaneda et al., 2002. As reported by Deal et al., 2000, a quasi-Yagi antenna is a compact and simple planar antenna that can operate over an extremely wide frequency bandwidth (of the order of 50%) with good radiation characteristics in terms of beam pattern, front-to-back ratio and cross-polarization. The compact size of the single element ($<\lambda_0/2$ by $\lambda_0/2$ for entire substrate) and low mutual coupling between the elements make it ideal for use in an array. The antenna is compatible for integration with microstrip-based monolithic-microwave-integrated circuits (MMICs).

The quasi-Yagi antenna is fabricated on a single dielectric substrate with metallization on both sides, as shown in Fig. 8. The top metallization consists of a microstrip feed, a broad-band microstrip-to-coplanar stripline (CPS) balun and two dipoles. One dipole is the driver element fed directly by the CPS and the second dipole (the director) is parasitically fed. The metallization on the bottom plane forms the microstrip ground, and is truncated to create the reflector element for the antenna. The driver on the top plane simultaneously directs the antenna propagation toward the endfire direction, and acts as an impedance-matching parasitic element. The driver element may also be implemented using a folded dipole to give greater flexibility in the design of the driver impedance value and to enable use on a liquid crystal polymer substrate (Nikolic et al., 2009; Nikolic et al, 2010).

For this application, the quasi-Yagi antenna is fabricated on an Alumina substrate with following specifications: dielectric thickness 127μm, metallization thickness 3μm, dielectric permittivity ε_r=9.9 and loss tangent, tan δ = 0.0003.

The single element is optimized using CST Microwave Studio to improve the return loss over a wide frequency bandwidth centred at 72 GHz. The antenna dimensions and schematic configuration are shown in Fig. 8. The total area of the substrate is approximately 2.5 mm by 3 mm.

The impedance bandwidth (defined as return loss greater than 10 dB) of the single element shown in Fig. 9a, calculated using CST Microwave Studio, extends from 50.1 – 81.4 GHz.

The co- and cross-polar radiation pattern for two principle planes at 72 GHz is shown in Fig. 9b. The realized gain of the single element is 5.4 dBi from 71 – 76 GHz.

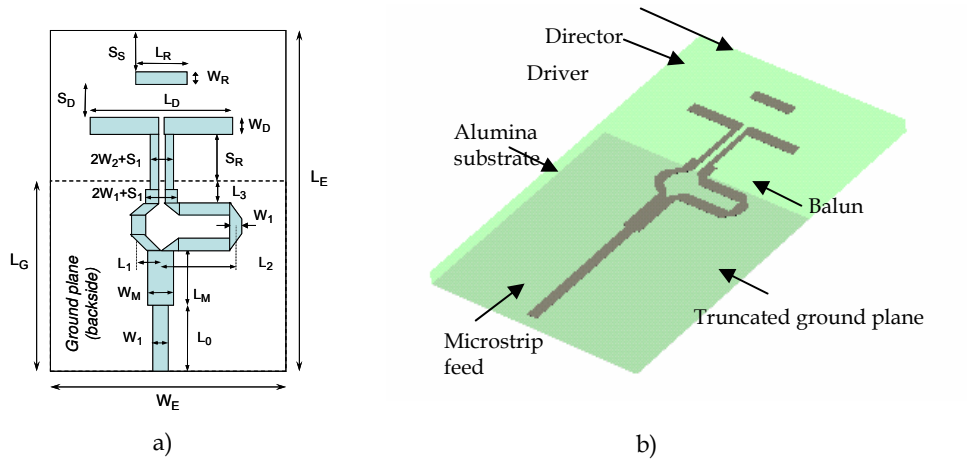

Fig. 8. Schematic of the quasi-Yagi antenna array element. L_E=3, W_E=2.5, W_1=0.12, L_0=0.45, L_G=1.54, L_M=0.54, W_M=0.205, L_1=0.22, L_2=0.7, L_3=0.1, S_1=0.06, W_2=0.06, L_D=1.29, L_R=0.488, W_D=0.12, W_R=0.12, S_R=0.516, S_D=0.323, S_S=0.383 (all dimensions in mm), substrate 127 um Alumina (ε_r=9.9, $tan\delta$=0.0003). b) Perspective view of a quasi-Yagi antenna

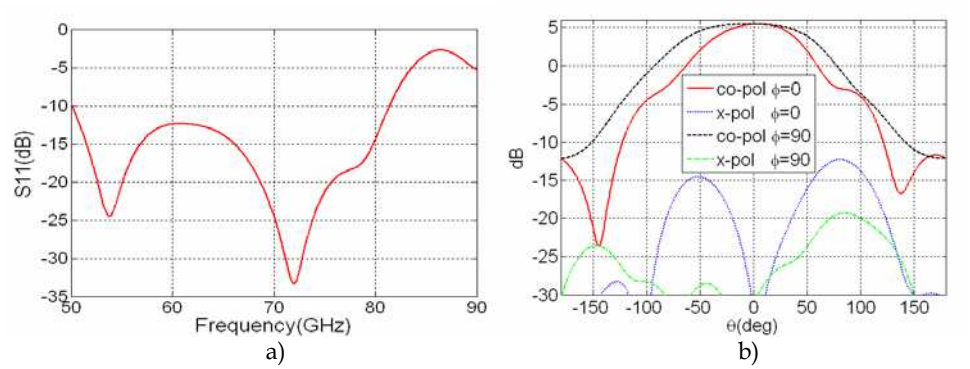

Fig. 9. a) Predicted reflection coefficient and b) radiation pattern at 72 GHz of the quasi-Yagi antenna shown in Fig. 8

6.2 Design of the arrays of quasi-Yagi antenna

The initial design of the four-element linear array was completed using the results for the radiation pattern of a single quasi-Yagi antenna multiplied by the array factor. The array factor is calculated assuming a linear array of equally spaced and uniformly excited elements. The spacing between the elements of $d=0.48\lambda_0$, shown in Fig. 10, was selected to minimise the appearance of grating lobes. The mutual coupling between the elements is presented in Fig. 11a.

The array factor for a uniformly excited four-element linear array with equal phase shift between each two consecutive elements is calculated from (Stutzman & Thiele, 1981)

$$AF = \frac{\sin(2\psi)}{\sin\left(\frac{1}{2}\psi\right)};\ \text{where}\ \ \psi = kd\cos\theta + \beta;\ \ k = \frac{2\pi}{\lambda_0}; \qquad 7)$$

The maximum of the array factor AF occurs for $\psi=0$. Let θ_m be the angle for which the array factor is maximal. Then, for the angle θ_m, measured from the line along which the array elements are placed, the required element-to-element phase shift β in the excitations is given by

$$\beta = -kd\cos\theta_m \qquad (8)$$

Assuming that the spacing between the elements is $d=0.48\lambda_0$, the required phase shift β is calculated using (2) and the results are summarized in Table 1.

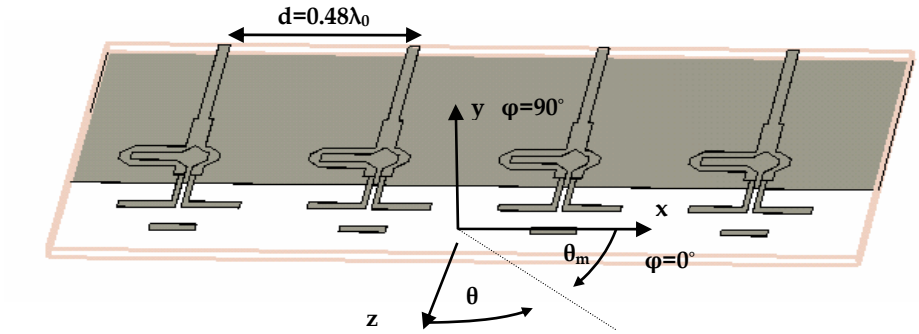

Fig. 10. Four-element linear array of quasi-Yagi antennas

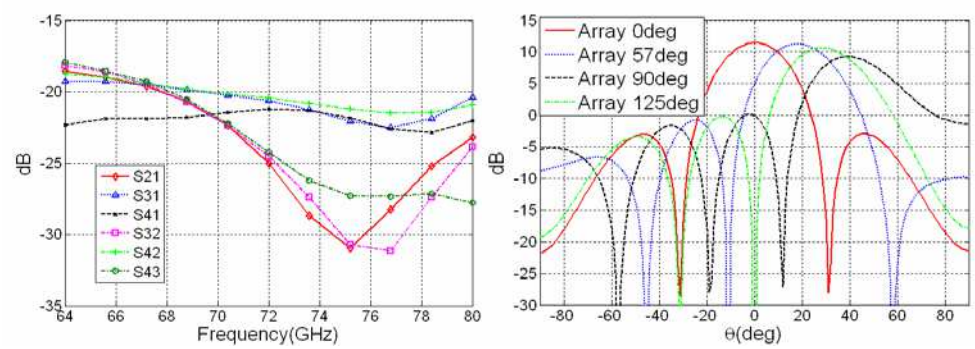

a) b)

Fig. 11. a) Calculated mutual coupling between elements of the four-element linear array shown in Fig. 10. b) Calculated radiation pattern of the four-element linear array for the φ=0° plane assuming different scanning angles

Array Description	θ	θ_m=90°- θ	β
Array 0deg	0°	90°	0°
Array 57deg	~20°	~70°	-57°
Array 90deg	~30°	~60°	-90°
Array 125deg	~40°	~50°	-125°

Table 1. The phase shift β between the array elements calculated using (2) and different angles θ_m

Using the values of the phase shift β, presented in Table 1, the radiation pattern of the four-element linear array is calculated in CST MWS and the results are shown in Fig. 11b. The next step was to design the microstrip feed networks to produce the required inter-element phase difference β, given in Table 1. Four microstrip feed networks were designed using simple T-junction power dividers and quarter-wavelength matching sections, as shown in Fig. 12.

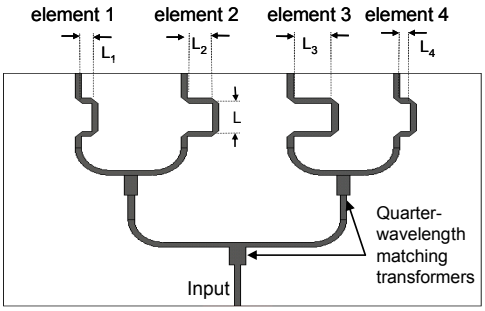

Fig. 12. Plan view of the microstrip feed network with equal amplitude and phase shift between the outputs

Three feed networks were designed to provide equal amplitudes at all elements and the element to element phase shift of β=57°, β=90° and β=125°. The required phase shift was achieved using microstrip lines L_1, L_2, L_3 and L_4, shown in Fig. 12 and for each array these lengths were optimized at 72 GHz. L=0.65 mm was selected for all arrays. For the array with the main beam pointing in the z-direction the feed network is designed using $L_1 = L_2 = L_3 = L_4 = 0$.

6.3 Microstrip-to-waveguide transition

In order to measure the network parameters and the radiation pattern of the array a suitable transition between the microstrip line and WR-15 waveguide has been optimized at 72 GHz. The configuration of the microstrip-to-waveguide transition is shown in Fig. 13a. Inner dimensions of the WR-15 waveguide are 3.76 mm by 1.88 mm, and its recommended operating frequency is from 50 GHz to 75 GHz. The important design parameters of the transition are the slot size in the waveguide wall, distance from the probe to the waveguide short-circuit, the length of the probe and the size of the rectangular cap at the end of the probe. Calculated results for the reflection and transmission coefficients are presented in Fig. 13b. Predicted return loss is better that 10 dB over the 60-80 GHz band and the transmission loss is less than 0.15 dB over the same band.

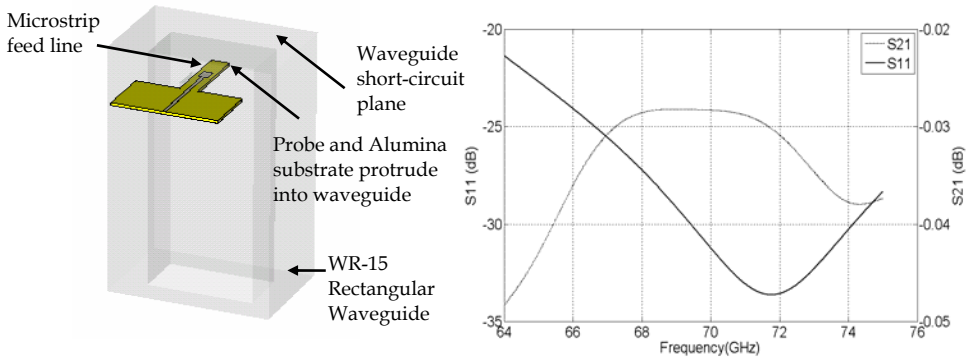

Fig. 13. a) Waveguide-to-microstrip transition b) Predicted reflection and transmission coefficients of the waveguide-to-microstrip transition

6.4 Measured results

Four separate linear quasi-Yagi arrays with integrated microstrip feed networks and microstrip-to-waveguide transitions were fabricated and tested. The layouts of two arrays are shown in Fig. 14.

The arrays were fabricated and bonded to the brass fixture blocks using conductive epoxy by the CSIRO Gigahertz Packaging Laboratory. The mechanical fixture design for the arrays is shown in Fig. 15a. Network measurements were undertaken from 68-76 GHz in the CSIRO Gigahertz Testing Laboratory using a HP 8510C VNA.

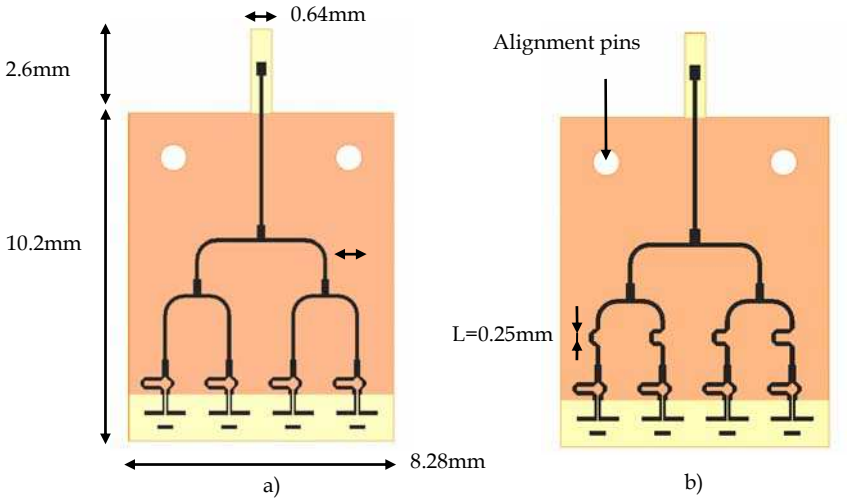

Fig. 14. Layouts of: a) Array-0°, and b) Array-57°

The measured reflection coefficients of the arrays are shown in Fig. 15b. For all arrays, the measured reflection coefficient was lower than -10 dB in the frequency bandwidth of 70.2-76 GHz.

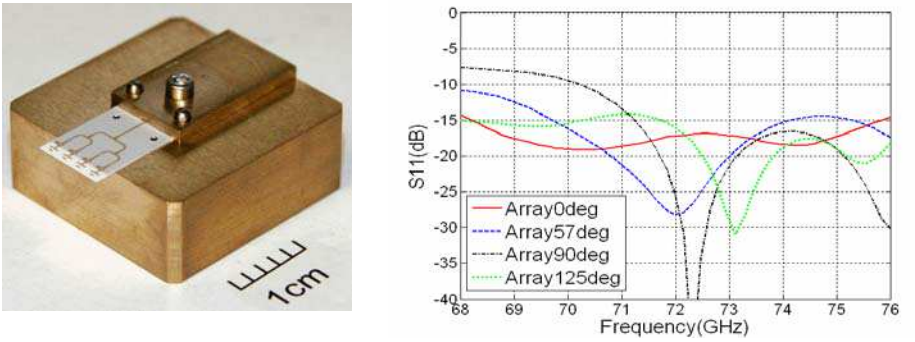

a) b)

Fig. 15. a) Photograph of a four-element linear array prototype integrated with a microstrip-to-waveguide transition. b) Measured reflection coefficients for all arrays

Radiation patterns and gain were measured in an anechoic chamber in CSIRO at 71.5 GHz, 72 GHz and 72.5 GHz. The radiation patterns were measured using a linearly polarized horn antenna at the transmitter. The simulated and measured co- and cross-polar radiation patterns of the array with the main beam in the broadside direction are shown in Fig. 16. Similar agreement between the simulated and measured results was achieved for the other three arrays and also at the other two frequencies.

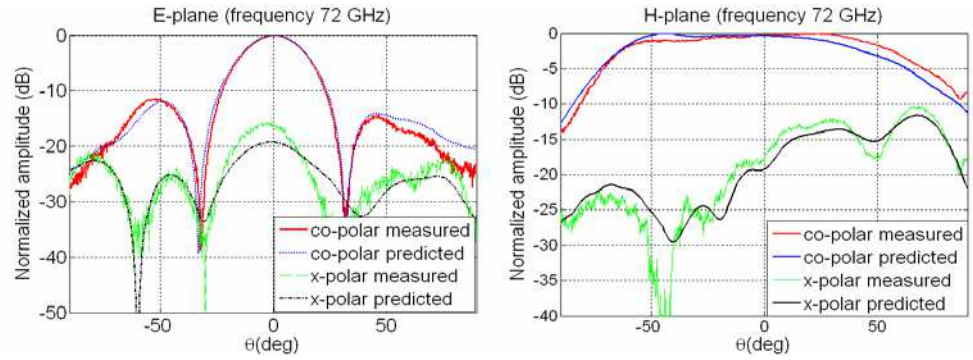

a) b)

Fig. 16. Measured radiation patterns of the Array-0deg at 72 GHz: a) E-plane and b) H-plane

Fig. 17 shows the measured normalized radiation patterns of the four arrays in the xz-plane. The side lobe levels may be improved by using a tapered excitation of the elements instead of the simple equal-amplitude excitation.

Computed and measured gain is compared in Fig. 18. The measured gain for all arrays is 8-9 dBi at 72 GHz, and the scan loss is about 1 dB. The measured gain for all arrays is about 1dB lower than the simulated results and this may be due to some additional losses in the microstrip-to-waveguide transition or higher losses in the dielectric material used for fabrication of the antennas.

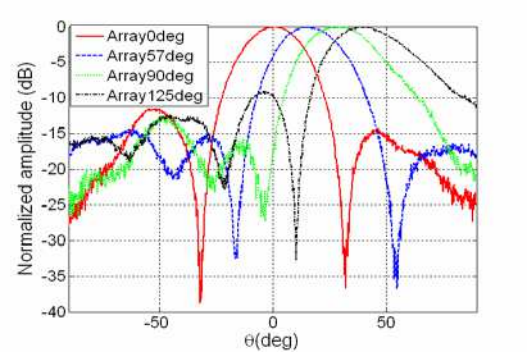

Fig. 17. Measured co-polar E-plane radiation patterns for all arrays at 72 GHz.

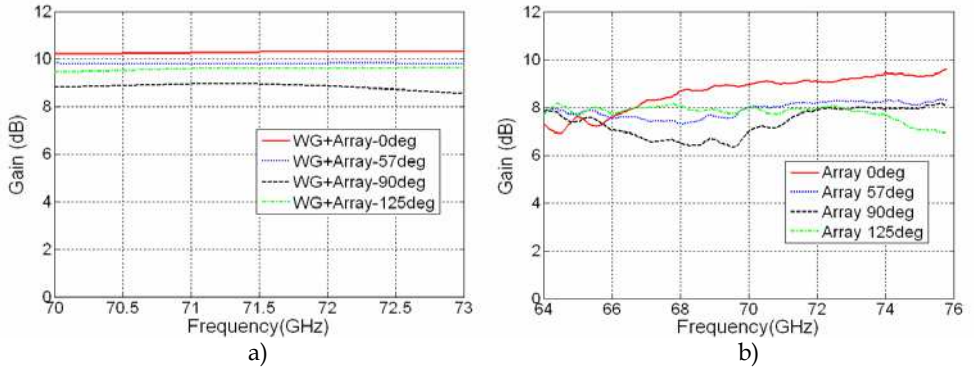

a) b)

Fig. 18. a) Calculated and b) measured gain for the four-element linear arrays

7. E-Band prototype test results

The analogue beam forming measurements were conducted in the CSIRO 12m far field anechoic chamber as shown in Fig. 19a where 1 is the receive array masked with absorbers, 2 is a rotator, 3 is the transmit antenna aperture and 4 is the de-modulator and power supply modules. Transmitter, digital modulator and control equipment were located on the outside of the chamber.

The available signal to noise ratio was above 33 dB for the measurement distance up to 6m, but most of the tests were conducted at the distance of 2.2m to minimize unwanted reflections from the walls and ceiling of the chamber.

The receive array has been calibrated by cancelling the main beam to obtain a null at zero degree azimuth angle. The calibration procedure was as follows. With one channel at a time active, magnitudes of all channel outputs were set equal. Then, with channel pairs active in the sequence 2-3, 1-2 and 3-4, phase weights were adjusted to null each pair. Then a 180 degree phase shift was applied to the null calibration reference settings to peak the main beam at 0° azimuth. Fig. 19b shows the E-plane array patterns measured for the null reference and the main beam steered to a 0° azimuth. Simulated data from CST Microwave Studio is shown for an array packaged in a waveguide test fixture depicted in Fig. 15a.

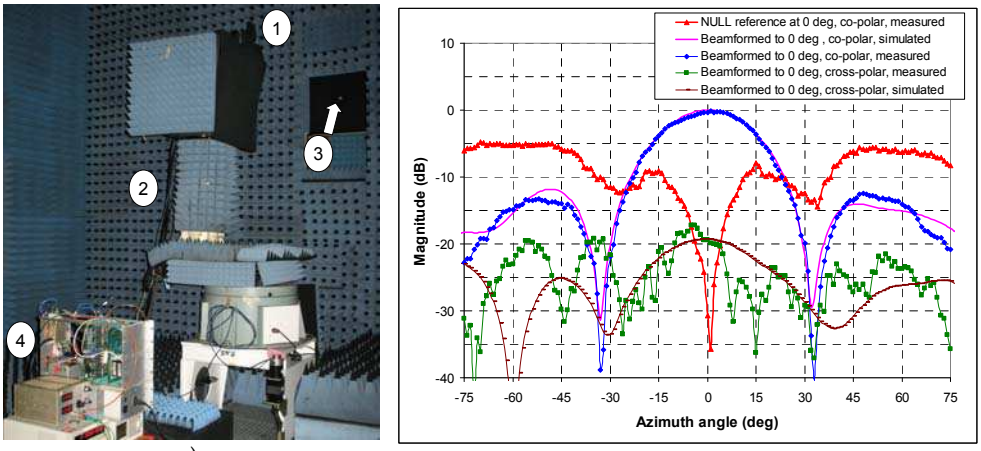

a) b)

Fig. 19. a) System test setup in the 12m far field anechoic chamber; b) Measured and simulated E-plane array co-polar and cross-polar patterns for the main beam formed at 0° azimuth and the measured pattern for the null calibration

Experiments were conducted to validate obtained phase and magnitude weights by cancelling the main beam at a selection of azimuth angles as shown in Fig. 20.

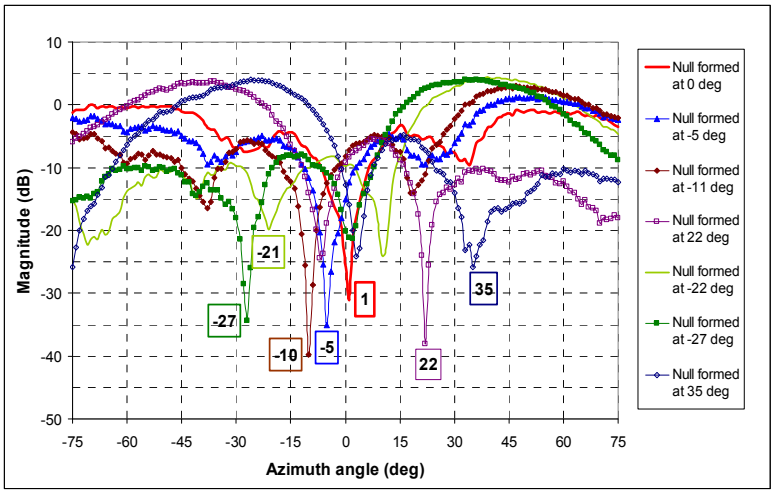

Fig. 20. Measured E-plane co-polar patterns for the array beam formed to cancel the main beam (form a null) at selected azimuth angle

Labels appended to each pattern show actual measured null positions. Experimental results were in a very close agreement with analytical estimates (≈ 1 degree). The array was steered to a selection of other positive and negative azimuth angles and E-plane antenna patterns were measured at each of the selected angles. The theoretical phase weights were applied to the null calibration reference settings to steer the beam to the non-zero azimuths. These

weights were calculated using the array factor formula for an uniformly excited array. Examples of measured E-plane co-polar antenna patterns are shown in Fig. 21 and Fig. 22.

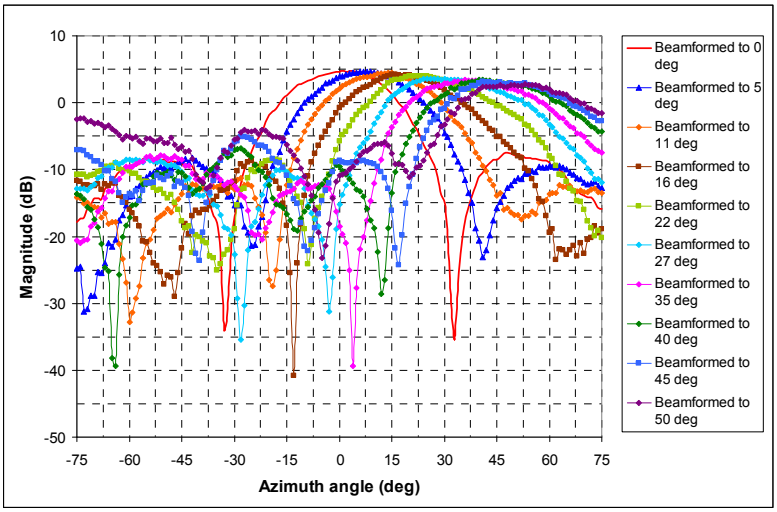

Fig. 21. Measured E-plane co-polar patterns for the array beam formed to a selection of positive azimuth angles

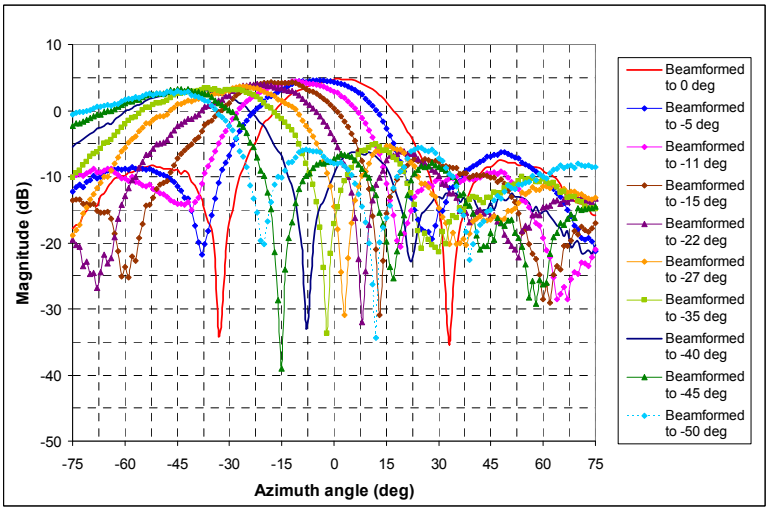

Fig. 22. Measured E-plane co-polar patterns for the array beam formed to a selection of negative azimuth angles

Cross-polar patterns have also been measured. A summary of the E-plane measurements is shown in Fig. 23. Measured antenna array patterns were very close to those predicted by the electromagnetic simulations (as described in Section 6) for steering angles ± 40°.

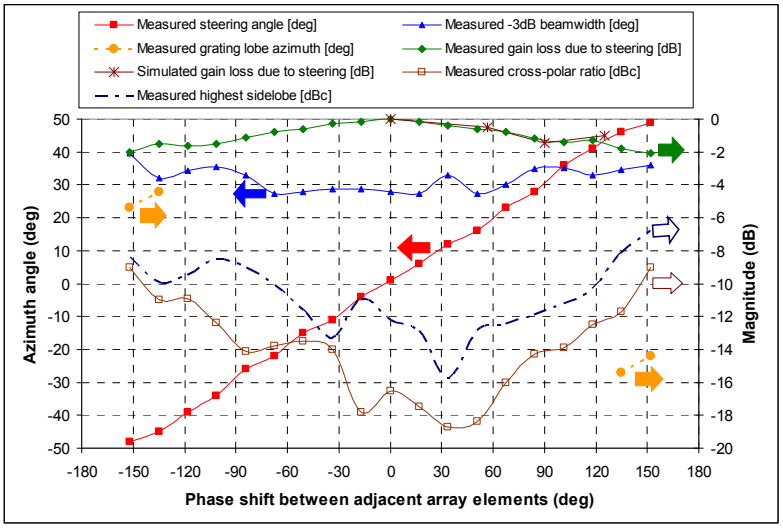

Fig. 23. Summary of the measurements

Measured array gain was 9.5dBi for steering angles below 22° and reduced to approximately 7.5dBi at the maximum steering angle of ± 42°. Grating lobes were observed only at the steering angles beyond ± 43°. Beam steering accuracy of 1 degree has been achieved with 6-bit digital phase shift and magnitude control at IF.

A small ad-hoc point-to-point link has also been tested with reasonable Bit Error Rate (BER) measured for selected angles using 8PSK modulation at 1.5 Gbps data rate. A single channel of the digital modem (Dyadyuk et al., 2007) was used for this experiment. The IF channel was centered at 1.5 GHz with the 625 MHz bandwidth and carried 1.5 Gbps Grey-coded 8-PSK pseudo- random noise sequences. Although pre-compensation (Dyadyuk et. al, 2007) reduces the residual BER, a dynamic pre-compensation would be required at different steering angles.

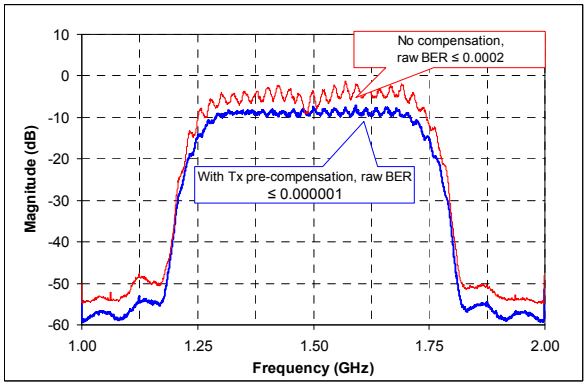

Fig. 24. Received signal at the output of A/D converter and measured BER for pre-compensated and un-compensated pseudo-random 8PSK symbols transmitted at 1.5 Gbps

Uncompensated transmit symbols used in this experiment for simplicity provided a reasonably low BER of 10^{-4}. In Fig. 24 the frequency response without signal pre-distortion (the upper trace) has a clear 3 dB ripple due largely to: a) mismatches between the Rx antenna outputs and the RF pre-amp inputs, and b) mutual coupling between the Rx antenna elements. Rx antenna s-parameters measurements indicated a return loss of 10 dB was to be expected with a 50 Ohm termination. Pre-distortion of the transmitted IF signal to cancel the distortion introduced by the RF transmission channels can be seen (the lower trace in Fig. 24) to reduce the ripples to 1.5 dB, and consequently reduce the 0-degree azimuth BER by a factor of 100.
Further improvement in BER would require better matching of the Rx antenna array and enhancement of the pre-compensation algorithm to better cancel the effects of mutual coupling.
A sample of measured raw BER at a selection of physical positions of the array and electronic steering angles is given in Table 2.

Array position (deg)	Scan angle, (deg)	Measured BER	Scan angle (deg)	Measured BER
-11	0	0.006	-11	0.0003
11	0	0.005	11	0.0002
-22	0	0.02	-22	0.0006
22	0	0.015	22	0.0005
-33	0	0.999	-33	0.001
33	0	0.99	33	0.009

Table 2. Measured raw BER at selected azimuth steering angles

8. Conclusion

In this chapter, we have presented a novel hybrid adaptive antenna array system for high data rate millimeter-wave ad-hoc wireless communications, and described hybrid digital beamforming algorithms.
The design of a single quasi-Yagi antenna element and four linear arrays has also been presented. The impedance bandwidth (return loss greater than 10 dB) of the single extends from 50.1 – 81.4 GHz and the realized gain is 5.4 dBi from 71 – 76 GHz. The arrays were designed and fabricated using quasi-Yagi antennas integrated with microstrip feed networks and suitable microstrip-to-waveguide transitions for testing. The feed networks were optimized to provide the required element-to-element phase shift between the antenna elements in order to point the main beam to the angles of 0°, 20°, 30° and 40°. The radiation patterns for all arrays were measured and excellent agreement between the simulated and measured results was achieved for the co- and cross-polar radiation patterns. The measured gain for all arrays is 8-9 dBi at 72 GHz, which is about 1 dB lower than the simulated results. For all arrays, the measured reflection coefficient is lower than -10dB in the frequency bandwidth of 70.2-76 GHz.
A steerable E-band receive array demonstrator that implements a four-element linear antenna array has been tested using analogue phase-only beam forming at IF. Measured array patterns were close to EM simulated estimates for steering angles up to ± 40 degree. Beam steering accuracy of 1 degree has been achieved with 6-bit digital phase shift at IF.

An ad-hoc wireless communication system has also been demonstrated. Reasonable BER was measured for an 8PSK data stream at 1.5 Gbps with the receive array beam formed in the direction of arrival of the transmit signal. To our knowledge, this work represents the first experimental results on a steerable antenna array in the E-band.

The developed demonstrator has also been used for experimental verification of the proposed wideband digital beam forming algorithms. Quantities analysis of the digital beamforming experiments is out of the scope of this chapter and can be found in (Dyadyuk et al., 20019c and Huang et al., 2010b).

Further work is focused on development of advanced multi-chip-module integration techniques for practical realization of tightly spaced mm-wave active antenna arrays and development of a larger 2D array prototype for experimental verification of the proposed hybrid beamforming algorithms.

9. References

Abbaspour-Tamijani, A. & Sarabandi, K. (2003). An affordable millimeter-wave beam-steerable antenna using interleaved planar sub-arrays. *IEEE Trans. Antennas & Propagation,* vol. 51, no. 9, Sept. 2003, pp. 2193-2202, ISSN: 0018-9480.

Deal, W. R; Kaneda, N.; Sor, J.; Qian Q.Y. & Itoh, T. (2000). A new quasi-Yagi antenna for planar active antenna arrays, *IEEE Trans. on Microwave Theory and Techniques*, Vol. 48, No. 6, June 2000, pp. 910-918, ISSN: 0018-9480.

Doan, C. H.; Emami, S.; Sobel, D. A.; Niknejad, A. M. & Brodersen, R. W. (2004). Design considerations for 60 GHz CMOS radios. *IEEE Communications Mag.,* vol. 42, no. 12, Dec. 2004, pp. 132-140, ISSN: 0163-6804.

Do-Hong, T. & Russer, P. (2004). Signal processing for wideband smart antenna array applications," *IEEE Microwave Magazine,* March 2004, pp. 57–67, ISSN: 1527-3342.

Dyadyuk, V.; Bunton, J. D.; Pathikulangara, J.; Kendall, R.; Sevimli, O.; Stokes, L. & Abbott, D. (2007). A multi-Gigabit mm-wave communication system with improved spectral efficiency," *IEEE Transactions on Microwave Theory and Techniques*, Vol. 55, No. 12, December 2007, pp. 2813–2821, ISSN: 0018-9480.

Dyadyuk, V.; Stokes, L. & Shen, M. (2008a). Integrated W-band GaAs MMIC Modules for Multi-Gigabit Wireless Communication Systems. *Proceedings of the 2008 Global Symposium on Millimeter Waves (GSMM 2008)*, April 2008, pp. 25-28, Nanjing, China ISBN: 978-1-4244-1885-5.

Dyadyuk, V.; Archer, J. W. & Stokes L. (2008b). W-Band GaAs Schottky Diode [MMIC Mixers for Multi-Gigabit Wireless Communications. *In: Advances in Broadband Communication and Networks, Agbinya, J. I. et al (Ed.),* 2008; Chapt. 4, pp. 73-103, River Publishers, ISBN: 978-87-92329-00-4, Denmark.

Dyadyuk, V. & Guo Y. J. (2009a). Towards multi-Gigabit ad-hoc wireless networks in the E-band. *Proceedings of Global Symposium on Millimeter Waves (GSMM 2009),* April 2009, pp.1-4, Sendai, Japan.

Dyadyuk, V.; Guo, Y. J. & Bunton, J. D. (2009b). Study on High Rate Long Range Wireless Communications in the 71-76 and 81-86 GHz bands. *Proceedings of the 39th European Microwave Conference (EuMC2009), Proceedings,* Sep. 2009, pp.1315-1318, Rome, Italy.

Dyadyuk, V.; Guo, Y. J. & Bunton J. D. (2010a). Enabling Technologies for Multi-Gigabit Wireless Communications in the E-band. *In: Fares, S. A & Adachi, F., eds. Mobile and*

Wireless Communications: Network layer and circuit layer design, In-TECH, 2010, Chapt. 13, pp. 263-280. ISBN: 978-953-307-042-01.

Dyadyuk, V. & Stokes L. (2010b). Wideband adaptive beam forming in the E-band: Towards a hybrid array. *Proceedings of Global Symposium on Millimeter Waves (GSMM 2010),* April 2010, Incheon, Korea.

Dyadyuk, V.; Huang, X.; Stokes L. & Pathikulangara J. (2010c). Implementation of Wideband Digital Beam Forming in the E-band: Towards a Hybrid Array. *Proceedings of the 40th European Microwave Conference (EuMC2010),* Sep. 2010, pp. 914 – 917, Paris, France.

Floyd, B.; Reynolds, S.; Valdes-Garcia, A.; Gaucher, B.; Liu, D.; Beukema, T. & Natarajan, A. (2007). Silicon technology, circuits, packages, and systems for 60-100 GHz, *IEEE MTT-S Intern. Microwave Symp. (IMS2007), Workshop WSN*, Honolulu, Hawaii, June 2007.

Goffer, A. P.; Kam, M. & Herczfeld, P. R. (1994). Design of phased arrays in terms of random sub-arrays. *IEEE Trans. Antennas Propagation*, vol. 42, no. 6, June 1994, pp. 820-826.

Gross, F. B. (2005). Smart *Antennas for Wireless Communications,* McGraw-Hill.

Guo, Y. Jay. (2004). *Advances in Mobile Radio Access Networks,* Artech House, Inc.

Guo, Y. J.; Bunton, J. D.; Dyadyuk, V. & Huang, X. (2009). Hybrid Adaptive Antenna Array. *Australian provisional patent,* AU2009900371, 2 Feb 2009.

Haupt, R. L. (2007). Optimized weighting of uniform sub-arrays of unequal sizes. *IEEE Trans. Antennas Propagation,* vol. 55, no. 4, Apr. 2007, pp.1207–1210.

Hirata, A.; Kosugi, T.; Takahashi, H.; Yamaguchi, R.; Nakajima, F.; Furuta, T.; Ito, H.; Sugahara, H.; Sato, Y. & Nagatsuma, T. (2006). 120-GHz-band millimeter-wave photonic wireless link for 10-Gb/s data transmission. *IEEE Trans. Microwave Theory Tech.*, vol. 54, no. 5, May 2006, pp. 1937–1044.

Huang, X.; Guo, Y. J. & Bunton, J. D. (2009). Adaptive AoA estimation and beamforming with hybrid antenna array of sub-arrays. *2009 IEEE Vehicular Technologies Conference (VTC 2009-Fall),* Sep 2009, Anchorage, Alaska, USA.

Huang, X.; Guo, Y. J. & Bunton, J. D. (2010a). A hybrid adaptive antenna array. *IEEE Transactions on Wireless Communications*, vol. 9, no. 5, 2010, pp. 1770-1779.

Huang, X.; Dyadyuk, V.; Guo Y. J.; Stokes, L. & Pathikulangara, J. (2010b). Frequency-Domain Digital Calibration and Beamforming with Wideband Antenna Array. *Globecom 2010,* Dec 2010, Miami, FL, USA.

Kaneda, N.; Qian, Q. Y. & Itoh, T. (1998). A novel Yagi-Uda dipole array fed by a microstrip-to-CPS transition, *Proceedings of Asia-Pacific Microwave Conf.*, Dec. 1998, pp. 1413-1416, Yokohama, Japan.

Kaneda, N.; Deal, W. R; Qian, Q. Y.; Waterhouse, R. & Itoh, T. (2002). A broad-band planar quasi-Yagi antenna*, IEEE Trans. on Antennas and Propagation*, Vol. 50, No. 8, August 2002, pp. 1158-1160, ISSN: 0018-926X.

Kasper, E.; Kissinger, D.; Russer P. & Weigel, R. (2009). High Speeds in a Single Chip. *IEEE Microwave Magazine*, Vol. 10, No. 7, Dec. 2009, pp. S28-S33, ISSN: 1527-3342.

Kosugi, T.; Hirata, A.; Nagatsuma, T. & Kado, Y. (2009). MM-Wave Long-Range Wireless Systems. *IEEE Microwave Magazine*, Vol. 10, No. 5, Apr. 2009, pp. 68-76, ISSN: 1527-3342.

Krim, H. & Viberg, M. (1996). Two decades of array signal processing research. *IEEE Signal Process. Mag.*, July 1996, pp. 67-94.

Lockie, D. & Peck, D. (2009). High-Data-Rate Millimeter-Wave Radios. *IEEE Microwave Magazine*, Vol. 10, No. 5, Aug. 2009, pp. 75-83, ISSN: 1527-3342.

Mailloux, R. J. (2005). *Phased Array Antenna Handbook,* Artech House, Inc.

Mailloux, R. J. (2007). *Sub-array technology for large scanning arrays. In Second European Conf. Antennas Propagation (EuCAP2007),* Nov. 2007.

Nikolic, N. & Weily, A. R. (2009). Printed quasi-Yagi antenna with folded dipole driver, *Proceedings of IEEE Antennas and Propagation Society (AP-S) International Symposium*, June 2009, Charleston, SC, USA.

Nikolic, N. & Weily, A. R. (2010). E-band planar quasi-Yagi antenna with folded dipole driver, *accepted for publication in IET Proceedings on Microwaves, Antennas and Propagation,* 2010, ISSN: 1751-8725.

Reynolds, S. K.; Floyd, B. A.; Pfeiffer, U. R.; Beukema, T.; Grzyb, J.; Haymes, C.; Gaucher, B. & Soyuer, M. (2006). A Silicon 60-GHz Receiver and Transmitter Chipset for Broadband Communications, *IEEE Journal of Solid-State Circuits*, Vol.41, Issue 12, Dec. 2006, pp.2820 – 2831.

Rogstad, D.; Mileant, A. & Pham, T. (2003). *Antenna Arraying Techniques in the Deep Space Network*. Wiley-IEEE.

Singh, H.; Oh, J.; Kweon, C. Y.; Qin, X.; Shao, H.-R. & Ngo, C. (2008). A 60 GHz wireless network for enabling uncompressed video communication. *IEEE Communications Magazine,* De. 2008, pp. 71–78, ISSN: 0163-6804.

Stutzman, W. L & Thiele, G. A. (1981). *Antenna Theory and Design*, John Wiley & Sons Inc., ISBN 0-471-04458-X, New York.

Vamsi, K.; Paidi, Griffith, Z.; Wei, Y.; Dahlstrom, M.; Urteaga, M.; Parthasarathy, N.; Seo, M.; Samoska, L.; Fung, A. & Rodwell, M. J. W. (2005). G-Band (140–220 GHz) and W-Band (75–110 GHz) InP DHBT Medium Power Amplifiers*", IEEE Transactions on Microwave Theory and Techniques*, Vol. 52, No. 2, Feb. 2005, pp. 598-605.

Wells, J. (2009). Faster than fiber: the future of multi-Gb/s wireless. *IEEE Microwave Magazine*, Vol. 10, No. 3, May 2009, pp. 104–112, ISSN: 1527-3342.

Xia, T.; Zheng, Y.; Wan, Q. & Wang, X. (2007). Decoupled estimation of 2-D angles of arrival using two parallel uniform linear arrays. *IEEE Trans. Antennas & Propagation*, vol. 55, no. 9, Sep. 2007, pp. 2627-2632.

Zirath, H.; Masuda, T.; Kozhuharov, R. & Ferndahl, M. (2004). Development of 60-GHz front-end circuits for a high-data-rate communication system. *IEEE J. Solid-State Circuits*, vol. 39, no. 10, Oct. 2004, pp. 1640-1649.

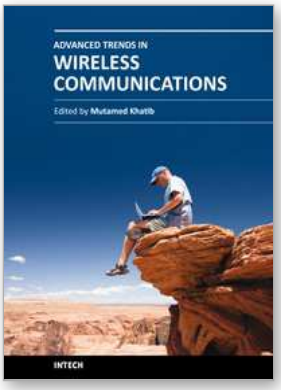

Advanced Trends in Wireless Communications

Edited by Dr. Mutamed Khatib

ISBN 978-953-307-183-1
Hard cover, 520 pages
Publisher InTech
Published online 17, February, 2011
Published in print edition February, 2011

Physical limitations on wireless communication channels impose huge challenges to reliable communication. Bandwidth limitations, propagation loss, noise and interference make the wireless channel a narrow pipe that does not readily accommodate rapid flow of data. Thus, researches aim to design systems that are suitable to operate in such channels, in order to have high performance quality of service. Also, the mobility of the communication systems requires further investigations to reduce the complexity and the power consumption of the receiver. This book aims to provide highlights of the current research in the field of wireless communications. The subjects discussed are very valuable to communication researchers rather than researchers in the wireless related areas. The book chapters cover a wide range of wireless communication topics.

How to reference

In order to correctly reference this scholarly work, feel free to copy and paste the following:

Val Dyadyuk, Xiaojing Huang, Leigh Stokes, Joseph Pathikulangara, Andrew R. Weily, Nasiha Nikolic, John D. Bunton and Y. Jay Guo (2011). Adaptive Antenna Arrays for Ad-Hoc Millimetre-Wave Wireless Communications, Advanced Trends in Wireless Communications, Dr. Mutamed Khatib (Ed.), ISBN: 978-953-307-183-1, InTech, Available from: http://www.intechopen.com/books/advanced-trends-in-wireless-communications/adaptive-antenna-arrays-for-ad-hoc-millimetre-wave-wireless-communications

INTECH
open science | open minds

InTech Europe
University Campus STeP Ri
Slavka Krautzeka 83/A
51000 Rijeka, Croatia
Phone: +385 (51) 770 447
Fax: +385 (51) 686 166
www.intechopen.com

InTech China
Unit 405, Office Block, Hotel Equatorial Shanghai
No.65, Yan An Road (West), Shanghai, 200040, China
中国上海市延安西路65号上海国际贵都大饭店办公楼405单元
Phone: +86-21-62489820
Fax: +86-21-62489821